ELSEVIER

Ceramics International 30 (2004) 525–532

CERAMICS INTERNATIONAL

www.elsevier.com/locate/ceramint

Role of a sodium glassy binder on microstructure and electrical conductivity of beta-alumina-based gas sensors

J.M. Tulliani [a,*], L. Dessemond [b], C. Esnouf [c]

[a] *Dipartimento di Scienza dei Materiali ed Ingegneria Chimica, Politecnico di Torino, Corso Duca degli Abruzzi 24, 10129 Torino, Italy*
[b] *Laboratoire d'Electrochimie et de Physico-Chimie des Matériaux Ioniques, CNRS-INPG-UJF, ENSEEG, B.P. 75, 38402 Saint Martin d'Hères, France*
[c] *INSA de Lyon, GEMPPM, CNRS UMR 5510, 20 Av. Albert Einstein, Villeurbanne, France*

Received 3 June 2003; received in revised form 22 June 2003; accepted 25 August 2003

Abstract

Interactions between β-Al_2O_3 and a sodium aluminosilicate conductive glass, after thermal treatment at 900 °C, have been investigated on screen-printed gas sensors. Due to the high level of glass additions, the starting powder made of β/β″-alumina, underwent strong compositional modifications. SEM and TEM imaging, coupled with chemical analysis, evidenced the formation of nepheline and α-Al_2O_3 at the interface between β-Al_2O_3 and the glass. Impedance spectroscopy measurements revealed that the higher the glass content, the larger was the conductivity decrease because of these microstructural changes.

Keywords: B. Electron microscopy; C. Electrical properties; C. Impedance; D. β-Al_2O_3; E. Sensors

1. Introduction

An original CO and NO_x sensor has been developed and patented some years ago [1] and was made of a β-Al_2O_3 pellet, on which two electrodes with different catalytic properties (one of gold, the other of platinum) were deposited. In the frame of a European project called Econox [2], this dense pellet was substituted by a screen-printed β-Al_2O_3 thick film having a maximum thickness of around 80 μm, in view of an industrial production. The firing temperature was low (900 °C) to avoid any loss of sodium from β-Al_2O_3. Since annealing temperatures of metallic electrodes in industrial processes are close to this value, a conductive sodium alumino-silicate glass has to be added to the sensing material, to achieve a good adhesion between the thick film and the substrate. Econox sensors thus contained 40 wt.% glass and the best compromise between adhesion, electrical response and durability in an exhaust flow was achieved with this composition. However, chemical reactions between β-Al_2O_3 and glass were clearly evidenced, and the aim of this work is to understand the nature, the location and the influence of additional phases on the electrical properties of the sensor. X-ray diffraction (XRD) and both conventional and high-resolution electron microscopy (TEM and HREM) were used for microstructural characterisation, while ac impedance spectroscopy was used to monitor the electrical conductivity of the system as a function of glass additions. Both transversal and longitudinal impedance measurements were performed on the same materials in order to check the consistency of the electrical characterisation.

2. Experimental procedure

Aluminium isopropoxide was hydrolysed in an aqueous solution of sodium oxalate at 80 °C, yielding an amorphous precipitate which was dried overnight at 105 °C [1]. Glass melt was obtained starting from Na_2CO_3, Al_2O_3 and SiO_2 powders and its softening temperature was around 780 °C. Mixtures of both powders were prepared in an alcoholic suspension in a planetary mill for 1 h (in agate jar with agate balls). Sensors were screen-printed on an α-Al_2O_3 substrate through a 325-mesh steel screen and all the samples were heat treated at 900 °C for 2 h, with a 2 °C/min heating

* Corresponding author. Tel.: +39-011-564-4700; fax: +39-011-564-4665.
E-mail address: jm.tulliani@netcourrier.com (J.M. Tulliani).

0272-8842/$30.00 © 2004 Elsevier Ltd and Techna Group S.r.l. All rights reserved.
doi:10.1016/j.ceramint.2003.08.001

ramp. More details on powders synthesis, pellets preparation, thick-films deposition and properties can be found elsewhere [1,3]. In this study, pellets of both pure β-Al_2O_3 and glass, and mixtures containing 10, 20, 40, 50 and 60 wt.% glass were prepared and labelled from now on as PX, where X represents the β-Al_2O_3 mass fraction. Only sensors with 60, 50 and 40 wt.% β-Al_2O_3 were screen-printed and referenced, respectively, S60 (Econox composition), S50 and S40.

XRD patterns were recorded in the 5–70° 2θ range on a Philips PW 1710 diffractometer at room temperature. Microstructural observations were performed with JEOL systems, a 840 series SEM, a 200 CX conventional TEM and a 2010 FEG-TEM for high-resolution imaging.

As screen-printed sensors are porous, a preliminary infiltration, under vacuum, with an epoxy-type adhesive was necessary prior to samples thinning, for TEM characterisation. The 400 μm α-Al_2O_3 substrate was then mechanically polished down to 100 μm, and then squares of 3 mm sides were cut and dimplered down to 20 μm, prior to argon ion milling (Gatan 691 Precision Ion Polishing System).

Gold paste electrodes (ESL 8835) were deposited, on one hand, on both sides of pellets referenced as TPX and, on the other hand, on the same side of samples (pellets or sensors) referenced as LPX or LSX. T and L stand, respectively, for transversal and longitudinal impedance measurements. Gold electrodes were subsequently fired in air at 500 °C for 2 h and at 600 °C for 1 h to remove volatile organic compounds. Two-point impedance measurements were performed in air between 200 and 650 °C (depending on the samples) in the 5–1.3×10^7 Hz frequency range (Hewlett-Packard 4192ALF impedance analyser). The magnitude of the ac measuring signal was varied between 100 and 500 mV to separate the sample impedance and the electrode characteristic. No impedance measurements were carried out on S40 sample.

The disappearance of the high frequency part of the diagram by increasing temperature made the resolution inaccurate typically beyond 300 °C for all investigated samples. As bulk contribution and blocking effects could not even be clearly separated at the highest measuring temperatures, a calculation of the corresponding activation energies (from linear regressions of the $\log(\sigma T)$ versus $1/T$ relationship) was thus omitted. The significant parameter used to describe the influence of the glassy phase on the recorded electrical properties is the total conductivity σ_t which was calculated from the low frequency intercept of the material impedance on the real axis in the Nyquist plane.

3. Results and discussion

3.1. Microstructural characterisation

The amorphous powder was heat treated at 1200 °C for 5 min, prior to mixing with glass, and XRD patterns (not shown here) revealed a mixture of β-, β′- and β″-Al_2O_3 (JCPDS cards 21-1095, 21-1096 and 19-1173, respectively). For the sake of clarity, sodium–beta-alumina based samples will be indicated, from now on, as β-Al_2O_3 without referring to the proportions of the different β-Al_2O_3 phases. The presence of both beta-alumina and nepheline ($NaAlSiO_4$, JCPDS card 35-0424) and traces of α-Al_2O_3 (JCPDS card 46-1212) were revealed from XRD on crushed pellets having different glass/beta-alumina contents. Peak intensities related to both former compounds are increasing function of the glass amount. In all pellets, total porosity was slightly affected by an increasing glass content and remained high (around 40 vol.%) [3]. EDX analysis, on pure glass deposited on an α-Al_2O_3 substrate, revealed that the glassy phase had the following composition: Na_2O, 19.1 wt.%; Al_2O_3, 12.3 wt.% and SiO_2, 68.6 wt.% and was quite homogeneous, after firing at 900 °C for 2 h. Accordingly, the nepheline formation can be regarded as resulting from the chemical reaction between beta-alumina and glass.

First SEM observations and EDX analysis on a fracture surface of a pellet containing 50 wt.% β-Al_2O_3 (P50)

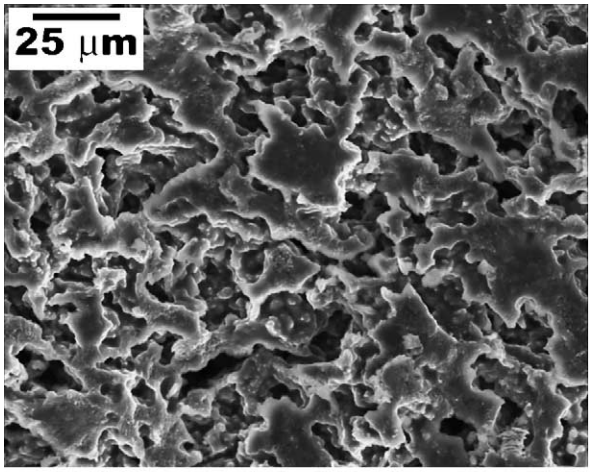

(a)

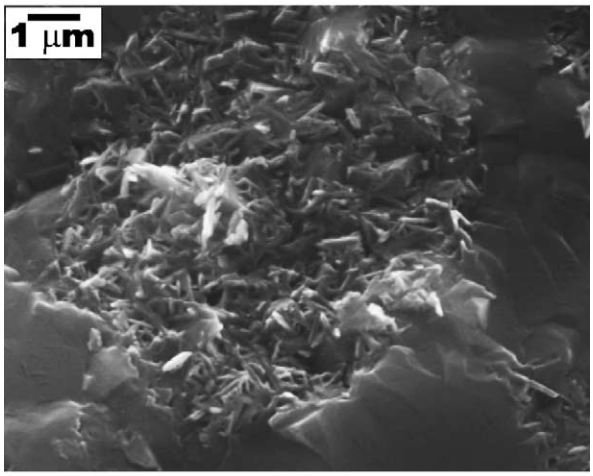

(b)

Fig. 1. SEM images of a β-Al_2O_3/glass sample interface (fracture surface of P50 sample).

indicated that samples were highly porous (Fig. 1a) and that beta-alumina platelets formed clusters (mean diameter of around 10 μm) surrounded by the glassy phase (Fig. 1b). The glass strongly adhered to these clusters but infiltrated them only in contact areas (Fig. 1b), yielding porosity inside the clusters.

EDX mapping on both P60 surface and two S40 sensors stuck together indicated that some isolated clusters made of only silica could be sometimes present (dotted circles in Fig. 2). This was probably a residue of unmelt silica powder during glass preparation process.

Conventional TEM observations showed that in all the samples, β-Al_2O_3 exhibited a hexagonal symmetry, looked like platelets of about 1 μm length and of 0.1 μm width. Its *c* axis is oriented perpendicular to the larger dimension of grains, which therefore corresponds to the conduction planes direction. Most of the grains were strongly faceted perpendicularly to this direction (Fig. 3). Diffraction patterns and chemical analysis of β-Al_2O_3 platelets confirmed the existence of the three phases β-, β′-, β″-Al_2O_3, in agreement with XRD investigations. Samples were composed of zones of a high concentration of beta-alumina pockets linked by glassy regions, as also illustrated by SEM observations (Fig. 1). Large nepheline crystals were located at the interface between β-Al_2O_3 platelets and glass, as illustrated by Figs. 4 and 5 for a sensor having 40 wt.% glass (S60). Concentric diffraction rings of Fig. 5 are typical of finely divided polycrystalline materials. A good agreement was achieved between the measured d_{hkl} values of Fig. 5 and the theoretical ones, according to JCPDS card 35-0424 (Table 1).

Table 1
Comparison between measured and theoretical d_{hkl} for nepheline crystals

Measured d_{hkl} (Å)	Theoretical d_{hkl} (Å)
6.08	6.00
4.98	4.99
4.37	4.32
4.32	4.28
4.17	4.16
3.81	3.83
3.73	3.75
3.32	3.27
3.23	3.20
3.09	3.04
2.91	3.00
2.87	2.88
2.74	2.72
2.70	2.64

HREM images recorded on a sample of same composition also confirmed the strong continuous interface between a β-Al_2O_3 rod and the surrounding glass (Fig. 6). Typical stacking faults due to sodium loss under electron beam were also evidenced in β-Al_2O_3 grains [4–6]. Small crystals of

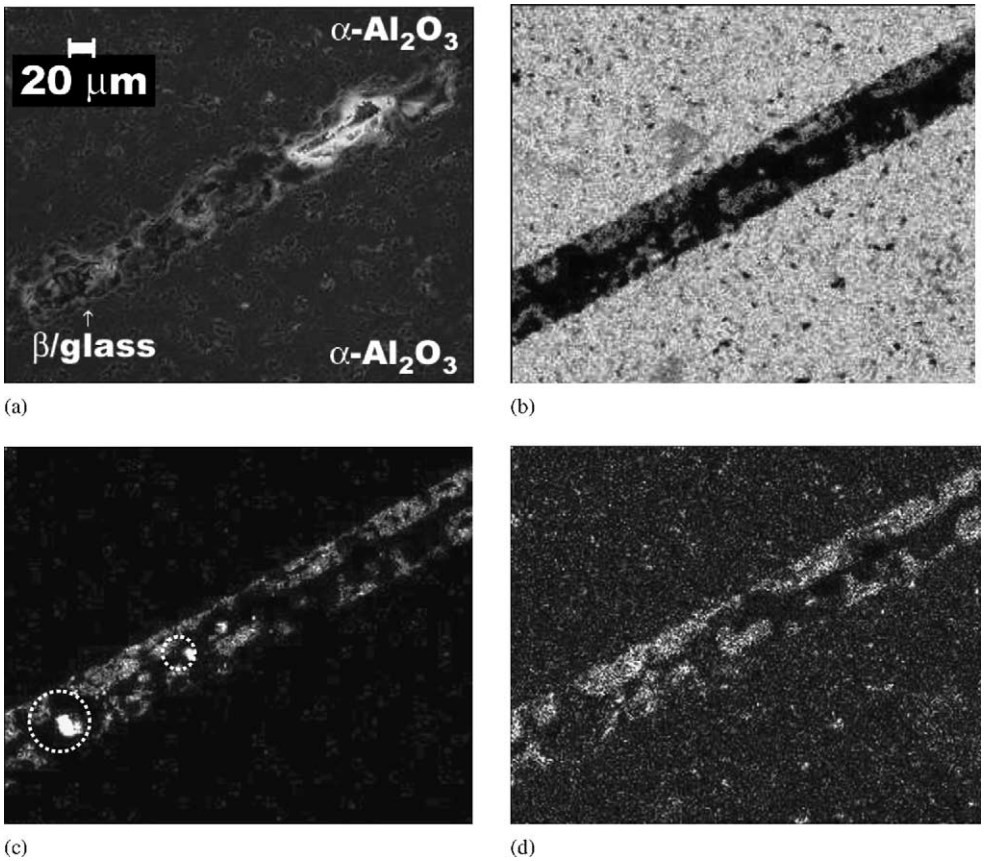

Fig. 2. SEM image of sensors (a) and EDX maps of Al (b), Si (c) and Na (d) (sample S40).

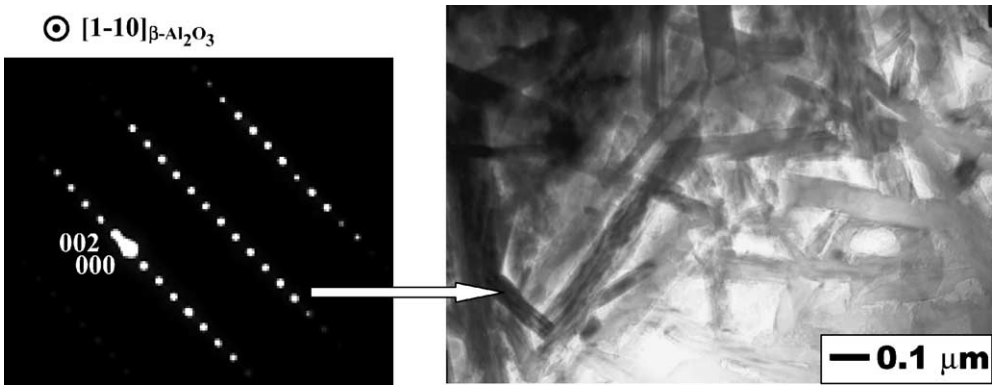

Fig. 3. TEM micrograph of β-Al_2O_3 grains pocket (sample S60) and corresponding diffraction pattern of a β-Al_2O_3 platelet.

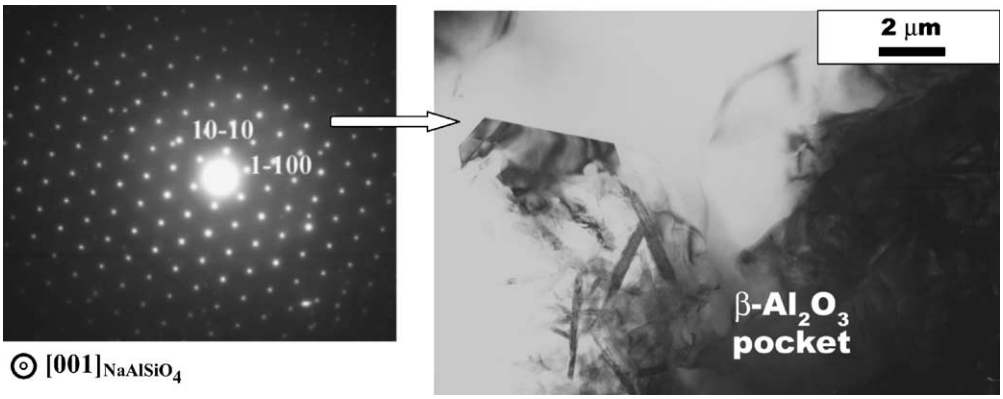

Fig. 4. TEM micrograph and corresponding diffraction pattern of a nepheline crystal close to a β-Al_2O_3 pocket (sample S60).

α-Al_2O_3, identified by EDX microanalysis and diffraction patterns, were found in the glassy phase as shown in Fig. 7. It was finally observed that glass composition strongly evolved during thermal treatment: silicon-rich regions were located close to beta-alumina clusters having a low sodium-content, while sodium- and aluminium-rich zones were found close to aluminium-rich crystals. This suggests that β-Al_2O_3 grains may act as sodium ions source for the glass, forming sodium rich pockets.

The highly heterogeneous microstructure of Econox sensors would be deleterious in the case of a bulk conduction mechanism but a new hypothesis concerning the sensors working conditions has been recently formulated [7]. The electromotive force of the sensor depends on the kinetic reactions which occur at each electrode in the same gas mixture. The charges are ascribed to the Na^+ species in the solid electrolyte and to the chemisorbed oxygen species on the metal. The charge distribution results in a capacitance effect

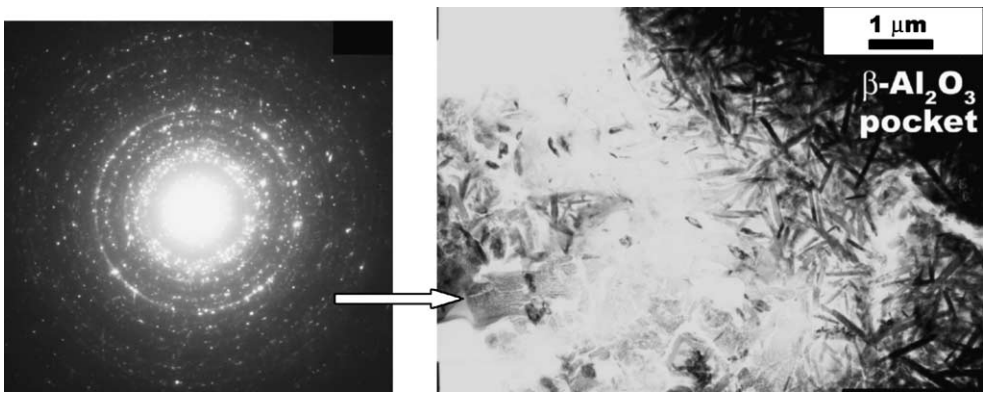

Fig. 5. TEM micrograph and corresponding diffraction rings of small nepheline crystals growing in β-Al_2O_3 pockets (sample S60).

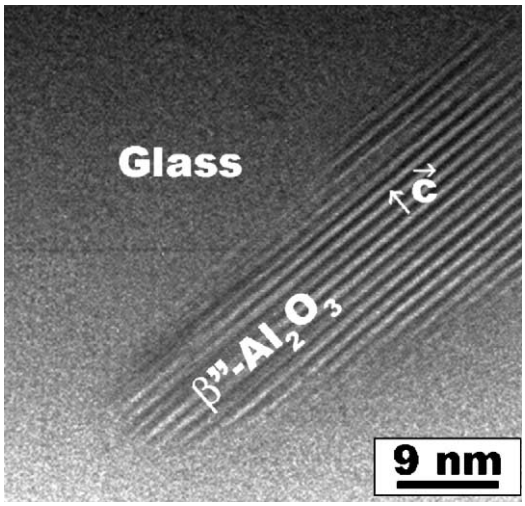

Fig. 6. HREM image of a β-Al_2O_3/glass interface (sample S60).

inside the electrolyte. In this scheme, the fact that β-Al_2O_3 loses Na^+ ions to the glass is positive and explains why these sensors appear to perform sufficiently well for use in selective CO and NO_2 detection in exhaust gases as a function of temperature [1].

3.2. Electrical characterisation

Whatever the measuring geometry, the inclined spike described typically below 10^2 Hz was ascribed to the electrode characteristic and the high frequency part of the diagram (beyond 10^2 Hz) was related to ionic conduction processes in the material (Fig. 8) [3]. The material impedance of sample LP100 could be properly resolved into two semicircles. For transversal measurements (sample TP100), the material impedance could be fitted only by one strongly depressed semicircle (depression angles of the order of 25–30°), but this simple decomposition was not regarded as specific of the related microstructure. It is noteworthy that the consistency of experimental results was not called into question by such a difference. For sample LP100, the high frequency (HF) and intermediate frequency (IF) semicircles were related to the bulk contribution of the material (intragrain contribution) and the blocking effect of conduction at pores between alumina grains, respectively [8]. Up to 300 °C, the magnitude of the IF semicircle represents 75% of the total resistance, but such a huge blocking effect is not in contradiction with previously published data [9,10]. This result confirms that the electrical properties of β-Al_2O_3 are determined more by the characteristics of microstructure defects than by those of the interior of grains [3].

Table 2
Activation energies of the total conductivity

Sample	$E(\sigma_t)$ (eV)
TP100	0.55
TP90	0.56
TP80	0.60
TP60	0.68
TP50	0.71
LP100	0.66
LP90	0.61
LP80	0.59
LP60	0.63
LP50	0.64
LS60	0.77
LS50	0.89

The values of total conductivity σ_t (Fig. 9) and corresponding activation energies $E(\sigma_t)$ (Table 2) determined for samples LP100 and TP100 are, respectively, lower and higher than those commonly reported in the literature [11,12] often determined for the high conductivity β″-phase [13]. The rather low conduction properties of samples TP100 and LP100 can be related to the electrical behaviour of the predominant β-phase within the measuring

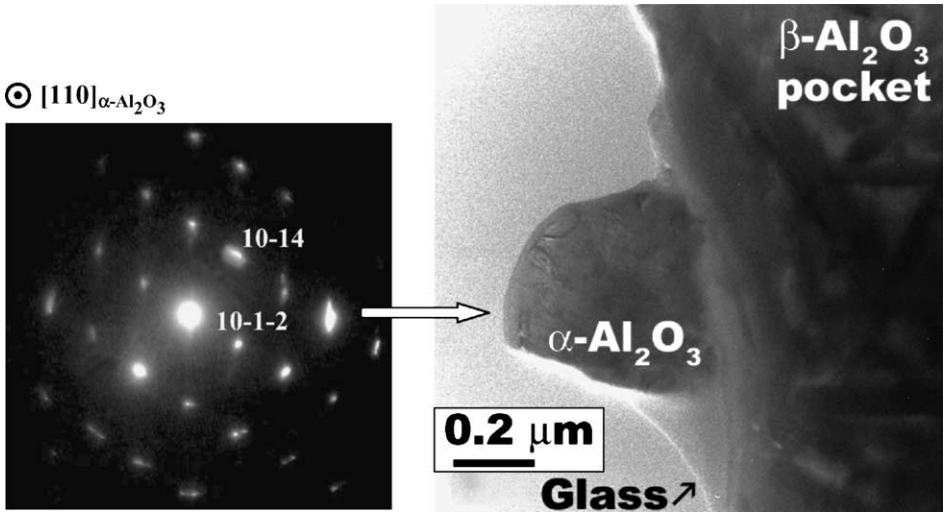

Fig. 7. TEM micrograph and corresponding diffraction pattern of a small α-Al_2O_3 crystal close to β-Al_2O_3 grains (sample S60).

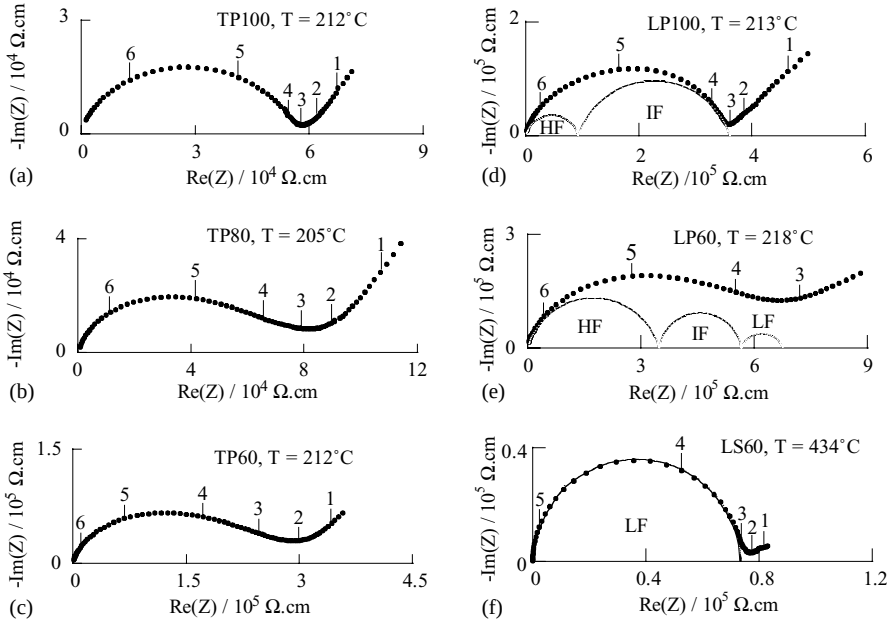

Fig. 8. Impedance diagrams recorded in air: (a)–(c) transversal and (d)–(f) longitudinal measurements. Numbers indicate the logarithm of the measuring frequency.

temperature range [14]. Moreover, the experimental values of $E(\sigma_t)$ are in the range of those calculated from molecular dynamics simulation for stoichiometric β-Al_2O_3 [15].

In this study, neither variation of both total conductivity and impedance diagram shape was detected for periods up to 4 days during isothermal treatments nor thermal hysteresis was recorded within the measuring temperature range. At this stage, the influence of water vapour on the electrical properties of β-Al_2O_3 samples [16,17] was not taken into account, as for mixed samples where β-alumina particles were embedded in a glassy phase and thus were not in direct contact with the atmosphere. It is worth emphasising on the role of water vapour on the electrical behaviour of the glassy binder. Preliminary impedance measurements performed on pure glass samples indicated that it is also a sodium ion conductor [3]. Since no hysteresis was evidenced on the Arrhenius diagram of σ_t for both glassy phase and mixtures containing up to 50 wt.% glass, one can infer that water vapour do not significantly influence the glass impedance response in the chosen experimental conditions.

A striking result is that σ_t values determined from transversal measurements are always higher than those calculated from the longitudinal method (Fig. 9). Regarding close activation energy values for pellets, the ratio of both conductivities is nearly constant within the measuring temperature range. As no hydratation process can be considered and because of lack of experimental evidences of surface composition changes, the most probable explanation is an underestimation of the geometric factor for longitudinal geometry, mainly due to a spreading of current paths deeper than expected below the measurement electrodes.

Whatever the measurement configuration, the total conductivity remained nearly unchanged up to 20 wt.% glass (Fig. 9). Magnitudes of both HF and IF semicircles were not strongly modified indicating that no significant microstructural evolution was detected within this glass content range.

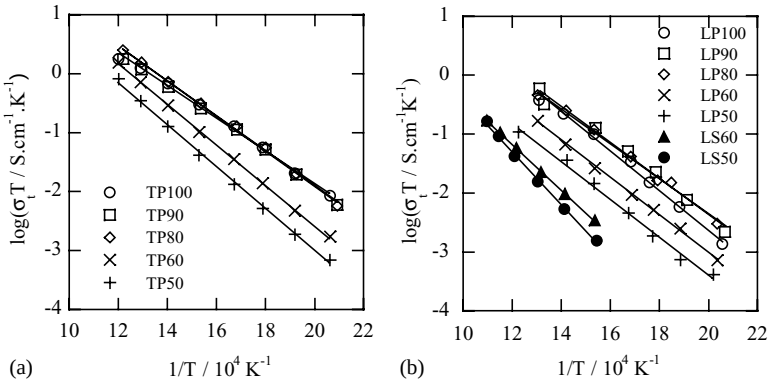

Fig. 9. Arrhenius diagrams of σ_t: (a) transversal and (b) longitudinal measurements.

Close activation energy values indicate that the conduction process was not strongly modified by adding the glassy phase (Table 2). However, the disappearance of the marked valley between the material impedance and the electrode characteristic at higher glass amounts indicates the contribution of an additional response (referenced as LF for low frequencies) whose magnitude is an increasing function of the glass content (Fig. 8). This results in lower conductivities for samples containing more glass (Fig. 9). According to the following discussion, this may result from a too low volume fraction of glassy phase. In spite of no accurate separation into individual responses, such a phenomenon is also clearly evidenced for transversal measurements.

Without any significant shift of the material impedance frequency distribution towards higher frequencies, the IF blocking effect in mixed pellets was attributed to a decreasing contact area between β-Al_2O_3 particles due to an increasing amount of the glassy phase [8]. Indeed, the HF conductivity of the glass is around five times lower than that of beta-alumina in the conditions of Fig. 8 [8]. Thus, the glassy binder can be regarded as insulating in comparison with the ceramic matrix. This is confirmed by the increasing magnitude of the IF semicircle for sample LP50 which represents 60% of the total resistance whereas 40% of it originates from this contribution for a mixed pellet containing 40 wt.% glass (Fig. 8). The large variations in chemical compositions of both β-Al_2O_3 and glassy phases at the alumina/glass interface as well as the presence of nepheline and α-Al_2O_3 within the mixed samples (Figs. 5 and 7) suggest that the LF semicircle can be related to the additional blocking effect of a thin insulating layer on average. This is in rather well agreement with the reference model of blocking effect in low-conductivity materials [18]. This approach predicts that the apex frequency (corresponding to the minimum of the imaginary part of the corresponding semicircle) of a blocking contribution is an increasing function of the average thickness, parallel to the applied electric field, of related microstructure defects: the higher the average thickness, the lower is the apex frequency. Another argument in favour of this assumption is that the HF conductivity is lower for samples LP60 and LP50 than for specimen LP100 (Fig. 8), as already reported for single crystalline Na^+–β″-Al_2O_3 with various degrees of ion exchange [12]. This would result in a lower charge carrier concentration, in agreement with chemical composition analysis.

The material impedance of thick films containing large amounts of glassy phase (LS60 and LS50 samples) is markedly different from those recorded on pellets (Fig. 8). The LF blocking effect becomes overwhelming and the activation energy of σ_t is even higher than that of pure glassy phase (0.74 eV) suggesting that ionic conduction is governed by another phase. A deleterious decrease of σ_t was also recorded (Fig. 9). This result further confirms the adverse effect of glass amounts higher than 40 wt.% on the total conductivity. For a permanent binder material, it seems essential to minimise the quantity of glass to preserve electrical behaviour close to those of beta-alumina while maintaining sufficient mechanical properties. Since a more homogeneous mixing of both β-Al_2O_3 and glassy phases can be achieved by using screen-printing, this would result in a larger wetting of β-Al_2O_3 grains. The cross sectional area of the insulating layer could be thus higher than in mixed pellets and this would yield a higher LF blocking effect in LSX specimens than in LPX ones (Fig. 8).

4. Conclusion

Glass additions to β-Al_2O_3 were necessary to prepare screen-printed sensors, however, this led not only to the formation of secondary phases, such as nepheline and small amounts of α-Al_2O_3 but this also strongly changed the sodium content inside β-Al_2O_3 agglomerates and in the residual glass, as clearly evidenced by SEM and TEM observations. This highly heterogeneous microstructure would be deleterious for the sensor in the case a bulk conduction mechanism based on β-Al_2O_3 grains. However, some positive experiments have been performed inside the Econox project to use pure glass sensors, even though their conductivity was low with respect to the mixed β-Al_2O_3/glass system.

Regardless of the measuring geometry, the adverse effect of a sodium aluminosilicate glass has been clearly evidenced from impedance spectroscopy measurements. The higher the glass content, the larger was the conductivity decrease. The degradation of electrical properties of mixed compounds was mainly due to the chemical reactivity between β-Al_2O_3 particles and the glassy phase. Up to 20 wt.% glass additions, the overall conductivities remained approximately constant, whatever the measuring configuration, while for higher glass amounts the contribution of an additional response was an increasing function of glass content. Conductivities calculated from transversal measurements, though higher respect to the longitudinal mode, probably because of an underestimation of the geometric factor in this second case, suggest that a surface conduction mechanism is possible and this is in agreement with the recently proposed hypothesis in the literature, for this kind of sensors. As Na^+ ions are responsible for conduction and as Na^+-rich pockets have formed after β-Al_2O_3 progressive collapse, there should be a percolation threshold, corresponding to samples with glass additions lower than 40 wt.%, associated with a change in the conduction regime from β-Al_2O_3 grains to Na^+-rich zones. This aspect has to be studied more in details and such samples have to be characterised. Nevertheless, up to 40 wt.% glass, the impedance of the mixed compound is nearly similar to that of β-Al_2O_3 in the vicinity of 700 °C.

References

[1] C. Pijolat, C. Pupier, C. Testud, R. Lalauze, L. Montanaro, A. Negro, C. Malvicino, Electrochemical sensors for CO/NO_x detection in automotive applications, J. Electroceram. 2/3 (1998) 181–191.

[2] Brite-Euram Contract, European Community, Project "Econox" n° BE-7058/1994–1997.
[3] J.M. Tulliani, L. Dessemond, L. Montanaro, P. Fabry, Preliminary investigations on the influence of a glassy phase on ionic conduction of beta-alumina, in: E.D. Wachsman, W. Weppner, E. Traversa, M. Liu, P. Vanysek, N. Yamazoe (Eds.), Solid State Ionic Devices, vol. II, Ceramic Sensors, The Electrochemical Society, Pennington, NJ, USA, 2001, pp. 79–89.
[4] L.C. De Jonghe, Planar [001] disorder in sodium beta alumina, J. Mater. Sci. 12 (1977) 497–502.
[5] L.C. De Jonghe, Spinel formation in sodium-β″-alumina, Mater. Res. Bull. 12 (1977) 667–674.
[6] J.O. Bovin, Blocking defects in β″-alumina observed by high resolution electron microscopy, Nature 273 (1978) 136–138.
[7] C. Pupier, J.C. Pijolat, J.C. Marchand, R. Lalauze, Oxygen role in the electrochemical response of a gas sensor using ideally polarizable electrodes, J. Electrochem. Soc. 146 (6) (1999) 2360–2364.
[8] J.M. Tulliani, L. Dessemond, P. Fabry, C. Esnouf, G. Fantozzi, Influence of glass content on microstructure and electrical conductivity of a β-alumina thick film, Key Eng. Mater. 206–213 (2002) 1223–1226.
[9] L.C. De Jonghe, Grain boundaries and ionic conduction in sodium beta alumina, J. Mater. Sci. 14 (1979) 33–48.
[10] G. He, T. Goto, T. Narushima, Y. Iguchi, Electrical conductivity of alkaline-earth metal b-aluminas and their application to a CO_2 gas sensor, Solid State Ionics 121 (1999) 313–319.
[11] E. Butchereit, M. Schreiber, J. Schoonman, Observations on the Na-β″-alumina/metal interface by impedance spectroscopy and scanning electron microscopy, Solid State Ionics 69 (1994) 1–12.
[12] F. Tietz, W. Urland, Impedance spectroscopy on Na^+/Ho^{3+}-β″-Al_2O_3 crystals, Solid State Ionics 78 (1/2) (1995) 35–40.
[13] G.W. Schäfer, A.P. de Kroon, F. Aldinger, Effect of aluminum raw materials on the formation of potassium-beta-aluminas, Solid State Ionics 81 (1/2) (1995) 43–51.
[14] H. Näfe, F. Meyer, F. Aldinger, Equilibrium between Na-β- and Na-β″-alumina as a function of the phase composition, Electrochim. Acta 45 (10) (2000) 1631–1638.
[15] J.V.L. Beckers, K.J. van der Bent, S.W. de Leeuw, Ionic conduction in Na^+-β-alumina studied by molecular dynamics simulation, Solid State Ionics 133 (3) (2000) 217–231.
[16] R.D. Armstrong, D.P. Sellick, A study into the effect of water vapour on sodium β-aluminas, Electrochim. Acta 25 (1980) 1199–1204.
[17] B. Dunn, Effect of air exposure on the resistivity of sodium beta and beta" aluminas, J. Am. Ceram. Soc. 64 (3) (1981) 125–128.
[18] M. Kleitz, L. Dessemond, M.C. Steil, Model for ion-blocking at internal interfaces in zirconias, Solid State Ionics 75 (1995) 107.